Vision, Modeling, and Visualization (2011)
Peter Eisert, Konrad Polthier, and Joachim Hornegger (Eds.)

Implicit Filtering for Image and Shape Processing

A. Belyaev[1] and H. Yamauchi[2]

[1]Heriot-Watt University, Edinburgh, Scotland, UK
[2]Sunday Research, Berlin, Germany

Abstract

The main purpose of this paper consists of demonstrating advantages of using implicit filtering schemes (non-causal IIR filters, in the signal processing language) for some basic image processing and geometric modeling applications. In particular, applications of implicit filtering for curve subdivision, image filtering, estimating image derivatives, and deblurring Gaussian blur are considered.

1. Introduction

Implicit finite differencing and filtering schemes constitute a powerful and widely used tool for accurate numerical simulations of physical problems involving linear and non-linear wave propagation phenomena [CL04], [PT05, Section 5.8], [LC09, Chapter 5]. Implicit finite difference schemes were considered by Collatz in his influential book [Col60] on numerical analysis of differential equations and implicit filters were studied by Raymond [Ray88, RG91] in relation with modeling weather phenomena. Widespread use of implicit finite differences and filters had been triggered by Lele [Lel92] who demonstrated their usefulness for computational problems with a range of spatial scales.

In the signal processing language, implicit filtering schemes correspond to noncausal infinite impulse response (IIR) filters. In image processing applications, finite impulse response (FIR) filters dominate over IIR image filtering schemes [Lim90, LA92] in spite of existence of highly computationally efficient implementations for the latter [DW97].

The main contribution of this paper consists of adapting implicit filtering schemes for uniformly-sampled univariate signals for image processing and shape modeling applications. In particular, applications of implicit filters for curve subdivision, image filtering, estimating image derivatives, and deblurring Gaussian blur are considered.

2. Implicit image filtering

Estimating image gradient. Given an image $I(x,y)$, the common way to estimate the first-order image derivatives consists of convolving $I(x,y)$ with kernel (mask)

$$D_x = \frac{1}{2h(1+2\alpha)} \begin{bmatrix} -\alpha & 0 & \alpha \\ -1 & 0 & 1 \\ -\alpha & 0 & \alpha \end{bmatrix} \qquad (1)$$

and its $\pi/2$-rotation. Here h is spacing between two neighboring pixels and, without loss of generality, we can assume that $h = 1$. Note that (1) can be decomposed into the product of standard central difference $[-1,0,1]/2$ in x-direction and smoothing $[\alpha,1,\alpha]/(1+2\alpha)$ acting in y-direction.

Let us take a brief look at stencil (1) from a frequency point of view. The eigenvalue (also called the frequency response) of (1) corresponding to the eigenfunction $\exp\{j(\omega_1 x+\omega_2 y)\}$, $j=\sqrt{-1}$, is given by

$$j\sin\omega_1 \frac{1+2\alpha\cos\omega_2}{1+2\alpha}, \quad -\pi<\omega_1,\omega_2<\pi,$$

where the first term of the product is the frequency response for the central difference and the second one corresponds to the smoothing kernel.

One can easily observe that the frequency response $j\sin\omega$ delivers a satisfactory approximation of $j\omega$, the frequency response for the ideal derivative, only for sufficiently small frequencies ω (see, for example, [Ham98, Section 6.4]). Now it is clear how (1) improves the standard central difference: smoothing introduced by the central difference is compensated by adding a certain amount of smoothing in the orthogonal direction. Such compensation leads to a more accurate estimation of the gradient direction while it adds smoothing to the gradient magnitude.

If an accurate estimation of both the gradient direction

DOI: 10.2312/PE/VMV/VMV11/277-283

and magnitude is required, one can combine differencing and smoothing in a different way. Namely, for each variable, let us combine finite differencing with inverted smoothing (sharpening). This simple idea leads us immediately to the concept of implicit finite differences. For example, the derivative of a one-dimensional signal $f(x)$ represented by its uniformly sampled values $\{f_i\}$ can be estimated by

$$\frac{1}{1+2\alpha}\left(\alpha f'_{i-1}+f'_i+\alpha f'_{i+1}\right)=\frac{1}{2}\left(f_{i+1}-f_{i-1}\right). \quad (2)$$

Here smoothing by $[\alpha,1,\alpha]/(1+2\alpha)$ compensates smoothing introduced by central differencing $[-1,0,1]/2$.

Now the question is how well (2) approximates the true derivative. In other words, one has to study how well

$$j\sin\omega\,\frac{1+2\alpha}{1+2\alpha\cos\omega}, \quad (3)$$

the frequency response function corresponding to (2) approximates $j\omega$, the frequency response of the true derivative, for $0\le\omega\le\pi$.

Following [Lel92], let us evaluate the quality of approximation by its *resolving efficiency*, the range of frequencies ω over which a satisfactory approximation is achieved. Since it is not possible to get a reasonably good approximation when ω is close to π, the frequency range for the optimization is often specified by $0\le\omega\le r\pi$ with some $0<r\le 1$.

The left image of Fig. 1 illustrates the resolving efficiency of (2), (3) for various values of α. Setting $\alpha=1/4$ delivers the highest possible approximation accuracy that can be achieved by (3) at a small vicinity of $\omega=0$ and corresponds to a fourth-order Padé approximation at $\omega=0$ [Lel92, Col60]. Its explicit counterpart was studied by W. G. Bickley [Bic48] who showed that (1) with $\alpha=1/4$ has asymptotically optimal rotation-invariant properties when grid spacing h tends to zero (or, equivalently, for $\omega\ll 1$).

The case $\alpha=3/10$ constitutes an implicit counterpart of the Scharr scheme [SKJ97, JSK99] which is given by (1) with $\alpha=3/10$. The Scharr filter delivers a more accurate approximation of the gradient direction than the classical Sobel filter (mask (1) with $\alpha=1/2$) and, as a result, is popular among computer vision researchers and practitioners [BK08, Chapter 6]. The first image of Fig. 1 demonstrates remarkable frequency-resolving efficiency of (2) with $\alpha=3/10$ which is natural to call the implicit Scharr scheme.

Although the image gradient (I_x,I_y) is a rotation-invariant quantity, its finite-difference approximations are not. For many image processing and computer vision applications, a correct estimation of the gradient direction $\arctan(I_y/I_x)$ is of primary importance.

It turns out that, for the same value of parameter α, explicit kernel (1) and implicit filter (3) produce remarkably similar results in estimating the gradient direction for low frequencies (ω_1,ω_2). Indeed, it is easy to see that (1) can be decomposed into product of (3) and averaging kernel

$$\frac{1}{(1+2\alpha)^2}\begin{bmatrix}\alpha^2 & \alpha & \alpha^2\\ \alpha & 1 & \alpha\\ \alpha^2 & \alpha & \alpha^2\end{bmatrix}$$

which only slightly affects low frequencies.

Fig. 2 shows results of our numerical experiments with sinusoidal grating

$$I(x,y)=\sin\left(x^2+y^2\right),$$

where x and y are ranging from -16 to 16 with step-size $h=0.1$. It means that the frequencies vary from 0 to 0.51 cycles/pixel. The images of the top row show gradient direction errors

$$\left|\arctan\left(I_y^{appr}/I_x^{appr}\right)-\arctan\left(I_y/I_x\right)\right|$$

calculated using various approximations of the gradient for each pixel. The images of the bottom row present gradient errors

$$\sqrt{(I_x-I_x^{appr})^2+(I_y-I_y^{appr})^2}$$

for various approximations of the gradient at each pixel. Comparing the images obtained using the Scharr ($\alpha=3/10$) and Bickley ($\alpha=1/4$) kernels (1) with their implicit counterparts justify our theoretical results and demonstrate advantages of using implicit schemes for gradient estimation.

Implicit low-pass and band-pass filters. Inspired by [Lel92] let us consider a simple one-parameter family of implicit low-pass filters

$$\frac{1}{1+2\alpha}\left[\alpha\hat{f}_{i-1}+\hat{f}_i+\alpha\hat{f}_{i+1}\right]=\frac{1}{2}f_i+\frac{1}{4}\left(f_{i-1}+f_{i+1}\right) \quad (4)$$

The corresponding frequency response function is given by

$$\mathcal{T}_\alpha(\omega)=\frac{1+2\alpha}{1+2\alpha\cos\omega}\,\frac{1+\cos\omega}{2} \quad (5)$$

Here we assume that $-1/2<\alpha<1/2$. Observe that (4) combines smoothing kernel $[1/4,1/2,1/4]$ with the inverse of

$$\frac{1}{1+2\alpha}\left[\alpha,1,\alpha\right]. \quad (6)$$

Note that $-1/2<\alpha<0$ makes (6) a sharpening filter while $0<\alpha<1/2$ turns it into a smoothing kernel.

It turns out that (5) belongs to the family of the so-called *implicit tangent filters* introduced by Raymond [Ray88, RG91] and described by their corresponding frequency response functions

$$\mathcal{T}_{\varepsilon,p}(\omega)=\left(1+\varepsilon\tan^{2p}\frac{\omega}{2}\right)^{-1},\quad p=1,2,3\ldots., \quad (7)$$

where ε and p are user-specified parameters. Namely, substituting $p=1$ and $\varepsilon=\frac{1-2\alpha}{1+2\alpha}$ in (7) gives (5). Monotonicity

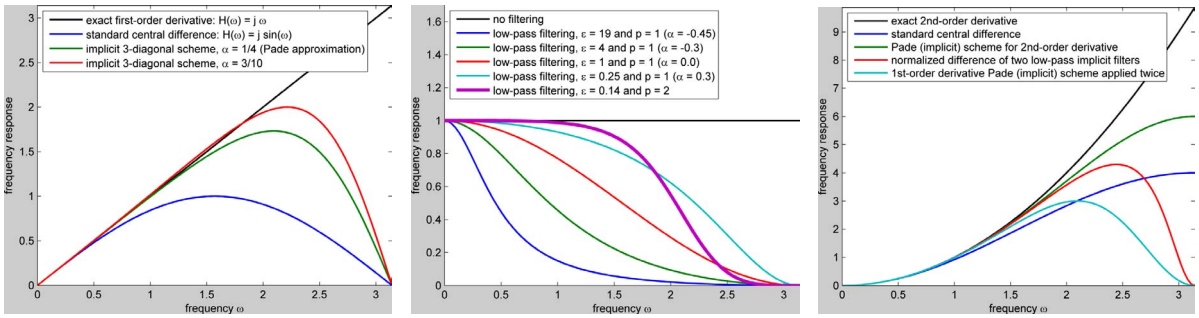

Figure 1: *Graphs of frequency response functions for various implicit filtering schemes. Left: various approximations of the first-order derivative operator. Middle: implicit tangent filters used for image deblurring (thick line) and curve subdivision (thin lines) examples considered in this paper. Right: various approximations of the second-order derivative operator. See the main text for further details.*

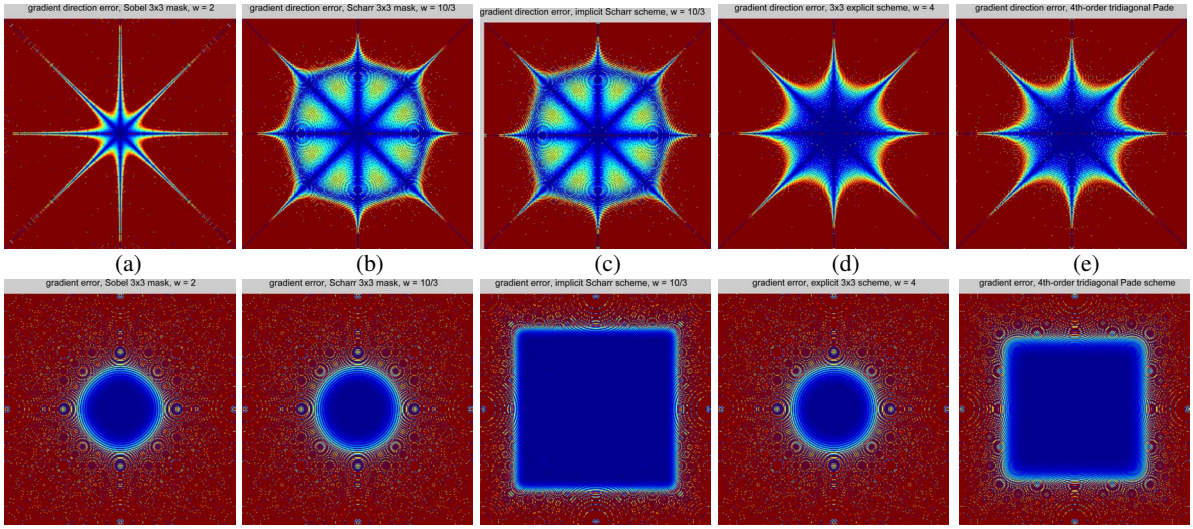

Figure 2: *Gradient direction (top row) and gradient (bottom row) errors calculated using various approximations of the gradient. Cooler color means higher accuracy. (a) Sobel kernel (1) with $\alpha = 1/2$. (b) Scharr kernel (1) with $\alpha = 3/10$. (c) Implicit Scharr scheme (2) with $\alpha = 3/10$. (d) Explicit filter (1) with $\alpha = 1/4$. (e) Implicit filter (2) with $\alpha = 1/4$. The Scharr kernel and implicit Scharr scheme deliver very similar gradient direction accuracy. Notice how good the implicit schemes are in estimating the gradient.*

of (7) for $0 < \omega < \pi$ and asymptotics

$$\mathcal{T}_{\varepsilon,p}(\omega) = \begin{cases} 1 - \varepsilon\,(\omega/2)^{2p} + O(\omega^{2p+2}) & \text{as} \quad \omega \to 0 \\ \frac{1}{\varepsilon}\left(\frac{\omega-\pi}{2}\right)^{2p} + O\left((\omega-\pi)^{2p+2}\right) & \text{as} \quad \omega \to \pi \end{cases}$$

justify remarkable properties of the implicit tangent filters.

The middle image of Fig. 1 displays the frequency response functions of several simple implicit tangent filters. These filters are used in image deblurring and curve subdivision examples considered in this paper.

One can easily verify that

$$\frac{(1+2\alpha)(1+2\beta)}{\beta-\alpha}\left[\mathcal{T}_\beta(\omega) - \mathcal{T}_\alpha(\omega)\right] \text{ with } \beta = \frac{1-\alpha}{1+8\alpha}, \quad (8)$$

where $0.1 < \alpha < 0.25$, corresponds to an accurate implicit approximation of the second-order derivative for low frequencies ω. In particular, the two limit cases $\alpha \to 0.25$ and $\alpha = 0.1$ correspond to the Padé scheme for the first-order derivative (implicit differencing (2) with $\alpha = 1/4$) applied twice and a similar Padé scheme for the second-order derivative

$$f''_{i-1} + 10 f''_i + f''_{i+1} = 12\,(f_{i+1} - 2f_i + f_{i-1})\,. \quad (9)$$

(see also [Col60, p. 538]), respectively. The right image of Fig. 1 displays graphs of the frequency response functions corresponding to (8). The main advantage of using (8) for estimating the 2nd-order derivative is that it is computationally efficient (solving three-diagonal systems of linear equations) and allows the user to control amount of smoothing needed for processing noisy signals.

It is also worth to note that (8) resembles the standard Difference-of-Gaussian (DoG) filter and, therefore, can be used for edge detection and non-photorealistic rendering purposes (see, for example, [Win06] where DoG was used for edge-based image enhancement and abstraction).

A different normalization of $\mathcal{T}_\beta(\omega) - \mathcal{T}_\alpha(\omega)$ yields a two-parametric family of band-pass filters. The normalization coefficient is found analytically and the resulting band-pass filters have low-computational complexity.

Stabilized inverse diffusion. Backward heat diffusion

$$\partial I/\partial t = -\Delta I, \quad I(x,y,t)|_{t=0} = I_0(x,y) \tag{10}$$

is a classical ill-posed problem and many inverse-diffusion regularization methods can be found in the literature [Pay75]. In particular, since the main source of instability in (10) consists of an exponential grow of high frequencies, it was proposed to stabilize (10) by suppressing high frequencies (low-pass filtering) [Sei96]. In [LK04], this natural approach was adapted for removing Gaussian blur from images.

It is also worth to note that Sobolev gradient flows [CMY10,CMY11,CM11] and closely related screened Poisson equation approach [BCCZ08] used for image sharpening exploit the same idea of suppressing high-order image frequencies.

Our regularization approach to (10) combines the forward Euler method with low-pass filtering

$$I(x,y,t+dt) = (\text{low-pass})\left[I(x,y,t) - dt\,\Delta_h I(x,y,t)\right]. \tag{11}$$

The low-pass filtering scheme we use employs implicit tangent filters defined by (7). As shown in [Ray88, RG91], for $p = 2$ the filters have a particulary simple form

$$(S+\varepsilon L)\cdot\begin{bmatrix}\hat{f}_{i-2}\\ \hat{f}_{i-1}\\ \hat{f}_i\\ \hat{f}_{i+1}\\ \hat{f}_{i+2}\end{bmatrix} = S\cdot\begin{bmatrix}f_{i-2}\\ f_{i-1}\\ f_i\\ f_{i+1}\\ f_{i+2}\end{bmatrix} \tag{12}$$

with $S = [1\ 4\ 6\ 4\ 1]$ and $L = [1\ -4\ 6\ -4\ 1]$. Despite of its simplicity, (12) maintains a relatively sharp cut-off transition.

Fig. 3 demonstrates our experiments with (11) and (12). We add blur using a discrete 7×7 kernel

$$K = \frac{1}{1003}\begin{bmatrix}0&0&1&2&1&0&0\\ 0&3&13&22&13&3&0\\ 1&13&59&97&59&13&1\\ 2&22&97&159&97&22&2\\ 1&13&59&97&59&13&1\\ 0&3&13&22&13&3&0\\ 0&0&1&2&1&0&0\end{bmatrix}$$

which approximates the Gaussian with $\sigma = 1$. The original image was convolved 25 times with kernel K, which is equivalent to adding Gaussian blur with $\sigma = 5$ and some noise due to discrete approximating the Gaussian kernel.

A good deblurring result was achieved after 75 iterations of (11), (12) with step-size $dt = 0.2$ and $\varepsilon = 0.14$ (see the middle image of Fig. 1 where the thick line visualizes the graph of the frequency response function corresponding to (12) with $\varepsilon = 0.14$). In theory, $\sigma^2/dt = 62.5$ iterations are needed to recover the original image. However discrete Laplacian Δ_h introduces some smoothing and, therefore, additional iterations of (11) are needed.

Very similar results are obtained if implicit filters proposed recently by J. W. Kim [Kim10] are used instead of (12).

We use (9) for approximating the second-order derivatives. According to our experiments, using standard explicit approximations of the Laplacian leads to slightly worse results since those approximations are less accurate for low and middle range frequencies ω than that obtained from (9).

3. Interpolation and curve subdivision

Subdivision of remains a hot research topic in computer graphics and geometric modeling [PR08, Sab10] (see also references therein). Below we establish simple links between implicit interpolation filters for uniformly sampled signals and implicit subdivision schemes.

Implicit subdivision schemes were introduced by Kobbelt in the case of interpolatory subdivision from a variational standpoint [Kob96, KS98, Kob98]. Unfortunately they were mostly forgotten: Sabin does not mention them at all in [Sab10] (although the key paper [Kob98] is listed the bibliography section) and Peters and Reif devoted to them only two sentences where the authors acknowledged their existence but wrongly stated that more or less nothing was known about the underlying theoretical properties of variational subdivision schemes [PR08] (see the last paragraph of [PR08, Section 9.2]).

In fact, [Kob98] contains mathematically rigorous and detailed analysis of variational subdivision schemes. The approach developed there can be used for studying theoretical properties of subdivision schemes considered below.

Figure 3: *Stabilized inverse diffusion for deblurring Gaussian blur. Left: original image. Middle: discrete Gaussian blur with* $\sigma = 5$ *is added. Right: deblurring by (11). See the main text for details.*

Implicit interpolation and interpolatory subdivision. Let us consider a simplified version of an implicit midpoint interpolation scheme introduced in [Lel92]

$$\alpha\hat{f}_{i-1} + \hat{f}_i + \alpha\hat{f}_{i+1} = \frac{a}{2}\left(f_{i-1/2} + f_{i+1/2}\right) + \frac{b}{2}\left(f_{i-3/2} + f_{i+3/2}\right) \tag{13}$$

The corresponding frequency response function is given by

$$H(\omega) = \frac{a\cos(\omega/2) + b\cos(3\omega/2)}{1 + 2\alpha\cos(\omega)}$$

One can easily observe that the famous four-point interpolatory subdivision scheme of Dyn, Levin, and Gregory [DLG87] is obtained from (13) when $\alpha = 0$ and $a = 1/16$, $b = -1/9$. Kobbelt's K_2 scheme [KS98] corresponds to $\alpha = 1/6$, $a = 4/3$, $b = 0$. Convergence and approximation properties of the interpolatory subdivision schemes corresponding to (13) follow from the spectral analysis technique developed in [Kob98].

In Fig. 4, we use four-times signal upsampling as a testing problem. Advantages of implicit interpolation/subdivision schemes over explicit ones are clearly demonstrated.

A family of implicit approximation subdivision schemes. Similar to implicit midpoint interpolation (13), we use implicit low-pass filters (4) for constructing approximation subdivision schemes. Given an initial control polygon $\left\{\mathbf{v}_i^{(0)}\right\}$, a sequence of subdivided polygons $\left\{\mathbf{v}_i^{(k)}\right\}$, $k = 1, 2, 3, \ldots$, is generated by

$$\mathbf{u}_{2i}^{(k)} = \mathbf{v}_i^{(k-1)}, \quad \mathbf{u}_{2i+1}^{(k)} = 1/2\left(\mathbf{v}_i^{(k-1)} + v_{i+1}^{(k-1)}\right),$$
$$\frac{1}{1+2\alpha}\left[\alpha\mathbf{v}_{i-1}^{(k)} + \mathbf{v}_i^{(k)} + \alpha\mathbf{v}_{i+1}^{(k)}\right] = \frac{1}{2}\mathbf{u}_i^{(k)} + \frac{1}{4}\left(\mathbf{u}_{i-1}^{(k)} + \mathbf{u}_{i+1}^{(k)}\right). \tag{14}$$

To the best of our knowledge, implicit approximation subdivision schemes have never been considered before. Fig. 5 demonstrates how parameter α, $-1/2 < \alpha < 1/2$, controls approximation properties of implicit subdivision scheme (14). See the middle image of Fig. 1 where graphs of the corresponding frequency response functions are plotted by thin lines.

We do not present here a convergence analysis of the family of implicit subdivision schemes corresponding to (4) since such an analysis can be done similar to that presented in [Kob98].

4. Conclusion

We hope that we clearly demonstrated advantages of using implicit filtering schemes for basic image and curve processing applications. We believe that the potential of implicit filtering schemes is largely underestimated and consider this work as an attempt to demonstrate usefulness of implicit filters for image processing and shape modeling purposes.

Some nontrivial issues that we have not touched in this paper include an appropriate treatment of boundary points (in this study, simple reflection boundary conditions are used for images and periodic bounary conditions are used for closed polygons), deriving implicit filtering schemes with high spectral resolution properties (see, for example, [Bel11] and references therein), and constructing implicit filtering schemes for irregularly sampled signals. These topics are widely studied in computational aeroacoustics [CL04] and their adaptation for image and shape processing purposes constitute an interesting theme for future research.

References

[BCCZ08] BHAT P., CURLESS B., COHEN M., ZITNICK L.: Fourier analysis of the 2D screened Poisson equation for gradient domain problems. In *European Conference on Computer Vision (ECCV)* (2008). 4

[Bel11] BELYAEV A.: On implicit image derivatives and their

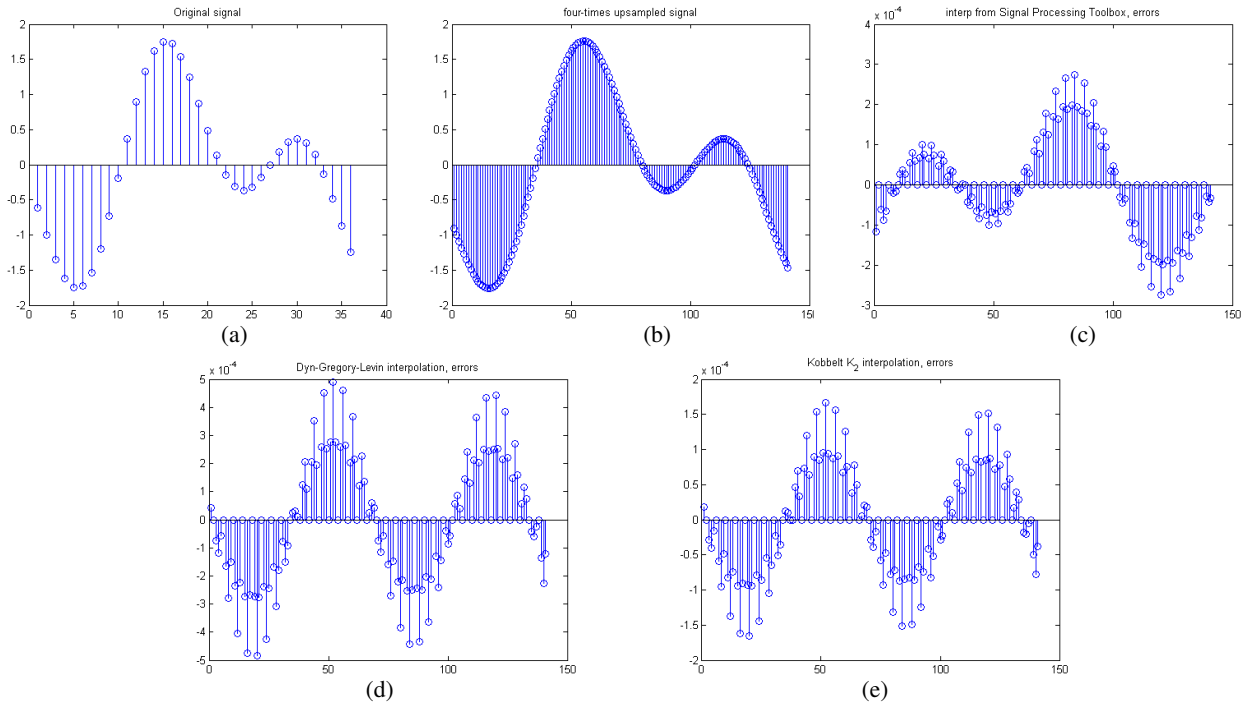

Figure 4: *Four-times upsampling. (a) Original uniformly-sampled signal. (b) Four-times upsampled signal. (c) Error introduced by Matlab's* `interp(x,4)` *function which uses a FIR filter with 34 entries; the maximal error is about* 3×10^{-4}. *(d) Error introduced by the Dyn-Levin-Gregory scheme, the maximal error is about* 5×10^{-4}. *(e) Error introduced by Kobbelt's* K_2 *scheme; the maximal error is about* 1.7×10^{-4}. *In this test, implicit* K_2 *scheme shows the best performance.*

applications. In *The 22nd British Machine Vision Conferenece (BMVC 2011)* (2011). 5

[Bic48] BICKLEY W. G.: Finite difference formulae for the square lattice. *Quart. J. Mech. Appl. Math. 1* (1948), 35–42. 2

[BK08] BRADSKI G., KAEHLER A.: *Learning OpenCV: Computer Vision with the OpenCV Library*. O'Reilly, 2008. 2

[CL04] COLONIUS T., LELE S. K.: Computational aeroacoustics: progress on nonlinear problems of sound generation. *Progress in Aerospace Sciences 40*, 6 (August 2004), 345–416. 1, 5

[CM11] CALDER J., MANSOURI A.: Anisotropic image sharpening via well-posed Sobolev gradient flows. *SIAM Journal on Mathematical Analysis* (2011). to appear. 4

[CMY10] CALDER J., MANSOURI A., YEZZI A.: Image sharpening via Sobolev gradient flows. *SIAM Journal on Imaging Sciences 3*, 4 (2010), 981–1014. 4

[CMY11] CALDER J., MANSOURI A., YEZZI A.: New possibilities in image diffusion and sharpening via high-order Sobolev gradient flows. *Journal of Mathematical Imaging and Vision 40*, 3 (2011), 248–258. 4

[Col60] COLLATZ L.: *The Numerical Treatment of Differential Equations*, 3rd ed. Springer, 1960. 1, 2, 4

[DLG87] DYN N., LEVIN D., GREGORY J.: A 4-point interpolatory scheme for curve design. *Computer Aided Geometric Design 4*, 4 (1987), 257–268. 5

[DW97] DANIEL M., WILLSKY A.: Efficient implementations of 2-D noncausal IIR filters. *IEEE Trans. on Circuits and Systems II 44*, 7 (July 1997), 549–563. 1

[Ham98] HAMMING R. W.: *Digital Filters*, 3rd ed. Dover, 1998. 1

[JSK99] JÄHNE B., SCHARR H., KÖRKEL S.: Principles of filter design. In *Handbook of Computer Vision and Applications, Vol. 2, Signal Processing and Applications*. Academic Press, 1999, pp. 125–151. 2

[Kim10] KIM J. W.: High-order compact filters with variable cut-off wavenumber and stable boundary treatment. *Computers & Fluids 39* (2010), 1168–1182. 4

[Kob96] KOBBELT L.: A variational approach to subdivision. *Computer Aided Geometric Design 13* (1996), 743–761. 4

[Kob98] KOBBELT L.: Using the discrete Fourier-transform to analyze the convergence of subdivision schemes. *Appl. Comp. Harmonic Anal 5* (1998), 68–91. 4, 5

[KS98] KOBBELT L., SCHRÖDER P.: A multiresolution framework for variational subdivision. *ACM Transactions on Graphics 17*, 4 (1998), 209–237. 4, 5

[LA92] LU W.-S., ANTONIOU A.: *Two-dimensional Digital Filters*. CRC Press, 1992. 1

[LC09] LI J., CHEN Y.-T.: *Computational Partial Differential Equations Using MATLAB*. CRC Press, 2009. 1

[Lel92] LELE S. K.: Compact finite difference schemes with spectral-like resolution. *Journal of Computational Physics 103* (1992), 16–42. 1, 2, 5

[Lim90] LIM J. S.: *Two-dimensional signal and image processing*. Prentice-Hall, 1990. 1

[LK04] LEE S.-H., KANG M. G.: Optimal regularized image

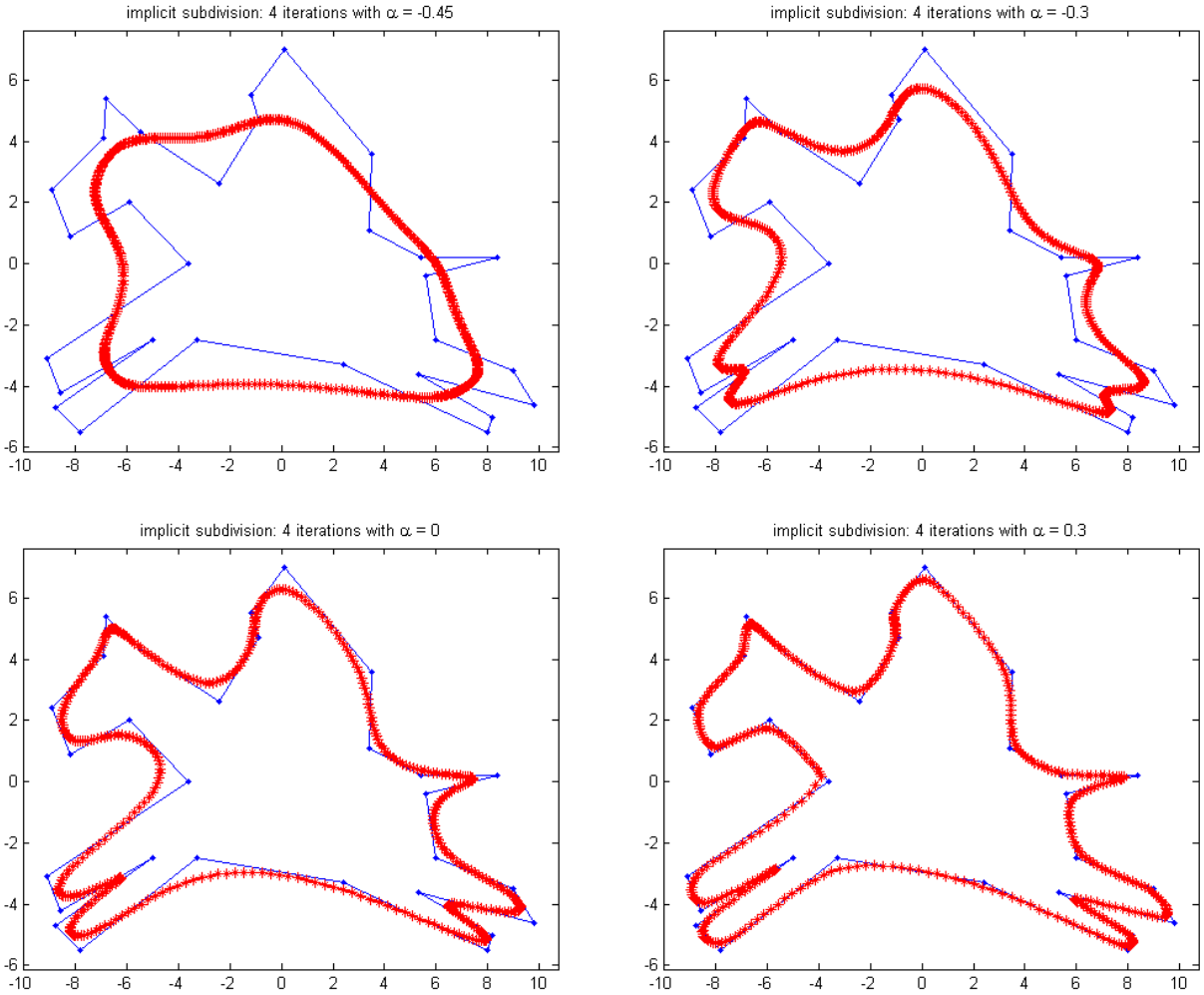

Figure 5: *Polygon subdivision by subdivision schemes corresponding to implicit low-pass filters (14). Top-left:* $\alpha = -0.45$. *Top-right:* $\alpha = -0.3$. *Bottom-left:* $\alpha = 0$. *Bottom-right:* $\alpha = 0.3$. *The parameter* α *in (14) controls the degree of approximation of the original control polygon* $\left\{\mathbf{v}_i^{(0)}\right\}$. *Graphs of the corresponding frequency response functions are shown in the middle image of Fig. 1 by thin lines.*

restoration algorithm based on backward diffusion equation. *Optical Engineering 43*, 1 (2004), 51–62. 4

[Pay75] PAYNE L. E.: *Improperly Posed Problems in Partial Differential Equations*. SIAM, 1975. 4

[PR08] PETERS J., REIF U.: *Subdivision Surfaces*. Springer, 2008. 4

[PT05] PETRILA T., TRIF D.: *Basics of Fluid Mechanics and Introduction to Computational Fluid Dynamics*. Springer, 2005. 1

[Ray88] RAYMOND W. H.: High-order low-pass implicit tangent filters for use in finite area calculations. *Monthly Weather Review 116* (1988), 2132–2141. 1, 2, 4

[RG91] RAYMOND W. H., GARDER A.: A review of recursive and implicit filters. *Monthly Weather Review 119* (1991), 477–495. 1, 2, 4

[Sab10] SABIN M.: *Analysis and Design of Univariate Subdivision Schemes*. Springer, 2010. 4

[Sei96] SEIDMAN T. I.: Optimal filtering for the backward heat equation. *SIAM J. Numer. Anal. 33* (1996), 162–170. 4

[SKJ97] SCHARR H., KÖRKEL S., JÄHNE B.: Numerische isotropieoptimierung von fir-filtern mittels querglättung. In *Proc. DAGM'97* (1997), pp. 367–374. 2

[Win06] WINNEMÖLLER: *Perceptually-motivated Non-Photorealistic Graphics*. PhD thesis, Northwestern University, Evanston, Illinois, USA, 2006. 4